ARTICLE

Low-cost synthesis of small molecule acceptors makes polymer solar cells commercially viable

Hongyuan Fu[1], Jia Yao[1], Ming Zhang[1], Lingwei Xue[1], Qiuju Zhou[2], Shangyu Li[1], Ming Lei [1], Lei Meng [3], Zhi-Guo Zhang [1✉] & Yongfang Li [3]

The acceptor-donor-acceptor (A–D–A) or A–DA'D–A structured small molecule acceptors (SMAs) have triggered substantial progress for polymer solar cells (PSCs). However, the high−cost of the SMAs impedes the commercial viability of such renewable energy, as their synthesis via the classical pyridine-catalyzed Knoevenagel condensation usually suffers from low reaction efficiency and tedious purifying work-up. Herein, we developed a simple and cheap boron trifluoride etherate-catalyzed Knoevenagel condensation for addressing this challenge, and found that the coupling of the aldehyde-terminated D unit and the A-end groups could be quantitatively finished in the presence of acetic anhydride within 15 minutes at room temperature. Compared with the conventional method, the high reaction efficiency of our method is related to the germinal diacetate pathway that is thermodynamically favorable to give the final products. For those high performing SMAs (such as ITIC-4F and Y6), the cost could be reduced by 50% compared with conventional preparation. In addition to the application in PSCs, our synthetic approach provides a facile and low-cost access to a wide range of D–A organic semiconductors for emerging technologies.

[1] State Key Laboratory of Chemical Resource Engineering, Beijing Advanced Innovation Center for Soft Matter Science and Engineering, Beijing University of Chemical Technology, 100029 Beijing, China. [2] Analysis & Testing Center, Xinyang Normal University, Xinyang 464000 Henan, China. [3] Beijing National Laboratory for Molecular Sciences, CAS Key Laboratory of Organic Solids, Institute of Chemistry, Chinese Academy of Sciences, 100190 Beijing, China. ✉email: zgzhangwhu@iccas.ac.cn

Polymer solar cells (PSCs) have drawn extensive research attentions in recent years, due to their advantages of light weight, flexibility, low-cost and large-area solution processing[1–4]. Recently, the power conversion efficiencies (PCEs) of PSCs have reached over 18%[5–11], which is mainly benefited from the emerging narrow-bandgap small molecule acceptors (SMAs) with attractive advantages of easily adjustable structures, strong absorption in the near–infrared region and lower photon energy loss during photocurrent generation[3,12–15]. With the PCE of PSCs approaching the commercially viable efficiencies, increased attention has been paid to the cost of the photovoltaic materials[16]. Recently, a variety of low-cost polymer donors, such as poly(thiophene-quinoxaline) derivatives[17], have been well developed that can work well with SMAs, Therefore, the bottleneck for the commercialization of the PSCs, from the cost point of view, is the design and synthesis of low-cost SMAs.

The narrow bandgap SMAs possess a typical acceptor-donor-acceptor (A–D–A) or A–DA'D–A molecular structure with aromatic-fused-ring D or DA'D-core, like ITIC[18] and Y6[19]. In the SMAs, the intramolecular charge transfer involving D–A interactions provide a powerful approach for tuning their absorption and energy levels, while the intermolecular interactions of the terminal A–units (the π–π stacking of the A–units) of the SMA offer the main electron channel in devices[5,20]. Regarding their synthesis, the SMAs are generally constructed with modular synthesis[21], by the conventional pyridine-catalyzed Knoevenagel condensation of the aldehyde-terminated aromatic D or DA'D fused-ring[22–24] with the activated methylene-based end-capping A-group[25–29], such as 1,1-dicyanomethylene-3-indanone (IC) and its derivatives. However, the classical Knoevenagel condensation in the synthesis of the SMAs usually suffers from low yields (20–80%), long heating period (5–12 h) at 60 °C, unavoidable by-product due to using excess of A units (4-6 equiv. relative to D or DA'D unit) and thus tedious purifying work-up. Such drawbacks leads to high cost of the SMAs which limits their commercialization in PSCs.

To address the challenge, we demonstrated a Lewis acid-catalyzed atom-economic green synthesis, and found that the coupling of the aldehyde-terminated D unit and the A-end groups could be quantitatively finished the reaction within 15 min via a boron trifluoride etherate (BF₃·OEt₂) promoted Knoevenagel condensation in the presence of acetic anhydride. With this procedure, a gram-scale preparation of the widely used SMAs was demonstrated with an easier workup. Also, this method is convenient for the synthesis of new SMAs, especially those with new A-end groups. Most importantly, for the high-performance SMAs (such as Y6), their synthesis cost could be reduced by about 50% compared with conventional preparation. Thus our work provide a greener, large-scale and low-cost synthesis of the SMAs with non-metal catalyst at room temperature, which are desirable for commercialization of PSCs.

Results

Design with Knoevenagel condensation. The application of D–A concept to construct tailor-made organic semiconductors has greatly promoted the progress of organic electronics[30], and various chemical strategies have been developed for their synthesis (Supplementary Fig. 1). Especially, Knoevenagel condensation holds a great potential for a greener and effective synthesis without toxic chemicals (such as tin compound) and without noble metal catalyst that usually used in the stille couple reaction. Herein, we mainly focus on improving Knoevenagel condensation for a facile synthesis of D–A or A–DA'D–A structured SMAs used in PSCs.

As an important classical reaction, Knoevenagel condensation, the coupling of carbonyl compounds with the active methylene groups typically carries out in the presence of a weak base as catalyst, such as pyridine[31]. And a variety of well-developed methodologies have been developed to promote such transformation, like using ionic liquid, Lewis acid or microwave irradiation. So far, the well-developed Knoevenagel condensation are mainly used in the synthesis of non-conjugated products, such as chemical intermediates, pharmaceuticals, cosmetics and perfumes[31]. In the field of organic semiconductors, such as the SMAs in PSCs discussed here, the carbonyl compounds and active methylene groups for the Knoevenagel condensation are extensively conjugated to tune their photovoltaic properties, thus inevitably causing steric hindrance of the aryl group and solubility issues in common polar solvents. In addition, due to the reversible nature of this condensation, large excess of the IC-based methylene groups (4-6 equiv. relative to D or DA'D unit) is usually required to push the reaction equilibrium in favor of the desired products. In this case, the IC-based methylene groups could self-condense and/or further react with the target Knoevenagel product[31,32]. Therefore, it is highly desirable to search for a more effective Knoevenagel condensation method for the synthesis of the organic semiconductors.

Given the high reaction activity of diacetate and its easier access from corresponding aldehyde[33–35], we proposed the idea of conducting the Knoevenagel reaction via the diacetate toward a convenient synthesis of organic semiconductors. It is noted that Sakai et al. pioneeringly conceived a one-pot procedure to afford Knoevenagel products with the assistance of acetic anhydride reactant and catalyst. This procedure is successful in providing a good yield of ca. 70% for most of the Knoevenagel products after column chromatography[36], suggesting an alternative route to promote the conventional Knoevenagel reaction. Despite the advantage, the promotion of the Knoevenagel reaction via a quantitative transformation under a short reaction time remains a major challenge in chemistry. In addition, metal-free protocol is more desirable for the synthesis of organic photovoltaic materials. Recently, it has been reported that the metal residue in the photovoltaic materials usually result in a poor device performance in PSCs[37,38]. To remove this concern, tedious purification by recrystallization, time-consuming column chromatography or multiple precipitation would inevitably increase the cost of the SMAs. After screening a variety of Lewis acid based catalysts, acid anhydrides and solvents in the Knoevenagel condensation, we found that BF₃·OEt₂ catalyst is remarkably highly effective as a non-metal catalyst in the synthesis of the SMAs via a quantitative and fast condensation of aromatic aldehyde with A-end groups even at room temperature.

Reaction optimizations. As a landmark SMA widely used in the PSCs, ITIC was selected as the model compound to conduct our investigation (Fig. 1 and Table 1)[18]. Although the conventional Knoevenagel condensation led to ITIC with a low yield of 21% in the initial report, the concept of constructing such A–D–A structured SMAs opened an avenue for designing state-of-the-art SMAs. In our case, Knoevenagel condensation was initially conducted with the corresponding aldehyde (ITIC–CHO) and two equivalences of IC end group in toluene in presence of acetic anhydride at 60 °C. Obviously, no reaction took place without any catalyst. Then, a variety of Lewis acid catalysts were examined, including LiOTf, SnCl₂, RuCl₃, AlCl₃, Yb(OTf)₃, FeCl₃, InCl₃ and GaCl₃. Among the Lewis acid catalysts, LiOTf, SnCl₂ and RuCl₃ were found to be ineffective for this condensation, most likely due to their poor capability in activating the aldehyde to form corresponding diacetate intermediate (entries 1-3, in Table 1).
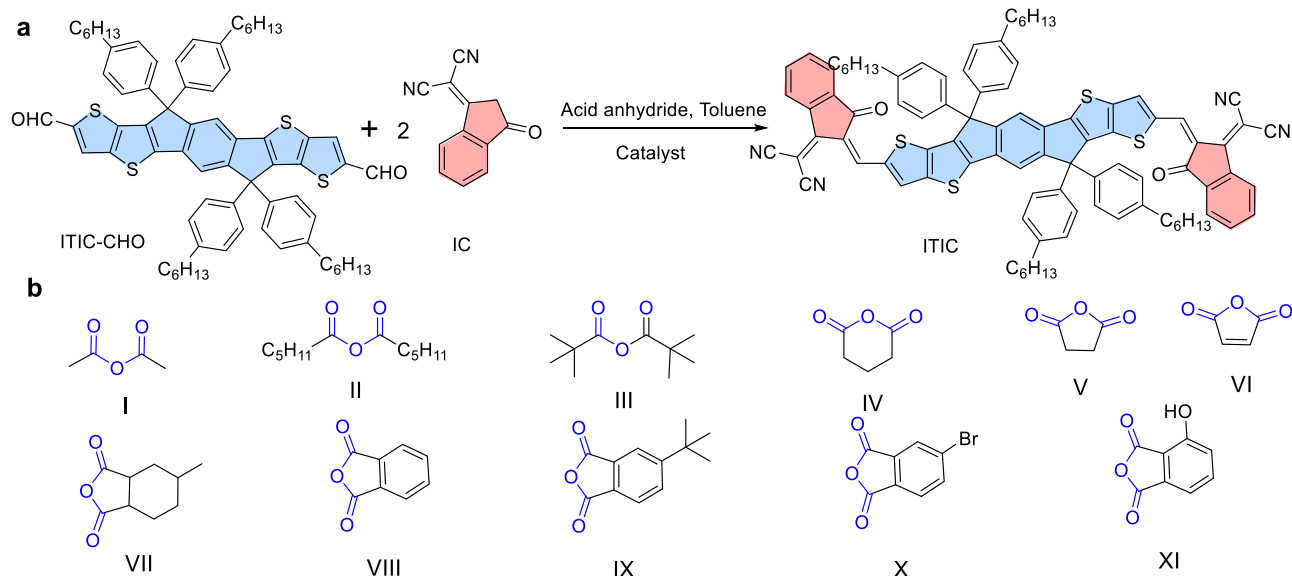
Fig. 1 The synthesis of SMAs. a The synthetic rout of ITIC, the bule color represents D unit and the red color represents the A unit. **b** The acid anhydrides explored, acid anhydride groups are indicated with blue color.

Table 1 The screening of the reaction conditions with metal catalysts for the synthesis of ITIC with 2 equiv. IC group[a].

Entry	Catalyst	Catalyst (mol %)	T (°C)	Time (min)	Yield[b] (%)
1	LiOTf	10	60	60	0
2	SnCl$_2$	10	60	60	0
3	RuCl$_3$	10	60	60	0
4	AlCl$_3$	10	60	60	0
5	Yb(OTf)$_3$	10	60	60	0
6	FeCl$_3$	10	60	60	0
7	InCl$_3$	10	0	60	10
8	InCl$_3$	10	30	60	64
9	InCl$_3$	1	60	300	20
10	InCl$_3$	2	60	300	32
11	InCl$_3$	5	60	125	>99%
12	InCl$_3$	8	60	80	>99%
13	InCl$_3$	10	60	40	>99%
14	InCl$_3$	15	60	30	>99%
15	InCl$_3$	20	60	30	>99%
16	GaCl$_3$	10	0	60	18
17	GaCl$_3$	10	30	88	80
18	GaCl$_3$	1	60	150	>99%
19	GaCl$_3$	2	60	80	>99%
20	GaCl$_3$	5	60	30	>99%
21	GaCl$_3$	8	60	13	>99%
22	GaCl$_3$	10	60	10	>99%
23	GaCl$_3$	15	60	9	>99%

[a]Reactions were performed with using ITIC-CHO and IC with a molar ratio of 1: 2;
[b]The yields were determined by ^{1}H NMR spectroscopy (400 MHz) with toluene-d$_8$ as an internal standard and solution.

For AlCl$_3$, Yb(OTf)$_3$ and FeCl$_3$, they showed poor catalytic performance, possibly due to their poor solubility in toluene (entries 4–6).

Notably, InCl$_3$ displayed good catalytic activity, while GaCl$_3$ proved to be a more effective catalyst as the reaction could complete within a shorter time or at a lower loading amount (entries 11–23 in Table 1). As shown in Table 1, the reaction rate using GaCl$_3$ as catalyst was 4 times faster than that using InCl$_3$ as catalyst. With higher loading amount of catalyst, the reaction could go to completion in a shorter period. From Supplementary

Fig. 2, it can be seen that there is a trade-off between reaction time and the concentration of the catalyst. Although reaction time can be shortened with a higher concentration of catalyst, which raised the concerns on the catalyst residuals. As a result, 5 mol % GaCl$_3$ was selected as the optimal loading amount, which led to full reaction conversion within 30 min at 60 °C (entry 20 in Table 1). The different catalytic activities between GaCl$_3$ and InCl$_3$ may be related to their molecular nature[39,40]. As shown in Supplementary Fig. 3, GaCl$_3$ adopts a bitetrahedral structure with two bridging chlorides. While for InCl$_3$, it features octahedrally coordinate In (III) center with close-packed chloride arrangement. As a consequence, GaCl$_3$ has a lower lattice energy, thus a better solubility (virtually all solvents) relative to that of InCl$_3$. The solubility is one plausible reason for the high catalytic activities of GaCl$_3$.

Despite the remarkable catalytic activity of GaCl$_3$, metal-free protocol is more desirable as metal residue is usually associated with the poor device performance as mentioned above. Encouragingly, we found that just with simple and cheap BF$_3$·OEt$_2$ as catalyst, higher catalytic activity was demonstrated (Table 2), even at room temperature (entries 2–6 in Table 2). Thus our approach provides a non-metal-catalyzed Knoevenagel condensation and an efficient method towards the synthesis of SMAs. Interestingly, we found that even when the reaction was performed at a low temperature of 0 °C, the reaction could also be completed within 80 min, suggesting a low-energy-consuming approach (entry 1).

Furthermore, different solvents, such as xylene, cyclohexane, pyridine, THF and CH$_2$Cl$_2$, were also screened for this GaCl$_3$ and BF$_3$·OEt$_2$-catalyzed transformation (Supplementary Table 1). It was found that xylene and CH$_2$Cl$_2$ were suitable for this reaction. However, cyclohexane, pyridine and THF led to no desired product. The low solubility of those conjugated substrates in cyclohexane should be the main reason for its ineffectiveness, while the weak coordination effect of GaCl$_3$ and BF$_3$·OEt$_2$ with the aldehyde substrate in pyridine and THF could explain why THF solvents were not applicable for this condensation. Besides BF$_3$·OEt$_2$, boron trifluoride tetrahydrofuran (BF$_3$·THF), boron trifluoride-acetic acid (BF$_3$·HOAc) and boron trifluoride acetonitrile (BF$_3$·CH$_3$CN) were also tested, they are as effective as that of BF$_3$·OEt$_2$ (entries 12–14 in Table 2). While for cyanuric

Table 2 The screening of reaction conditions with organic catalyst for the synthesis of ITIC with 2 equiv. IC group in toluene[a].

Entry	Catalyst	Catalyst (equiv[b])	T (°C)	Time (min)	Yield[c] (%)
1	$BF_3 \cdot OEt_2$	5	0	60	>99%
2	$BF_3 \cdot OEt_2$	5	28	15	>99%
3	$BF_3 \cdot OEt_2$	1	28	30	>99%
4	$BF_3 \cdot OEt_2$	2	28	20	>99%
5	$BF_3 \cdot OEt_2$	8	28	10	>99%
6	$BF_3 \cdot OEt_2$	10	28	5	>99%
7	$BF_3 \cdot OEt_2$	1	60	10	>99%
8	$BF_3 \cdot OEt_2$	2	60	8	>99%
9	$BF_3 \cdot OEt_2$	5	60	5	>99%
10	$BF_3 \cdot OEt_2$	8	60	5	>99%
11	$BF_3 \cdot OEt_2$	10	60	5	>99%
12	$BF_3 \cdot THF$	5	28	15	>99%
13	$BF_3 \cdot HOAc$	5	28	15	>99%
14	$BF_3 \cdot CH_3CN$	5	28	15	>99%
15	Cyanuric chloride	10	60	60	0
16	Carbon bromide	10	60	60	0
17[d]	Pyridine	15	60	720	22
18[e]	Pyridine	15	60	360	83

[a]Reactions were performed using ITIC-CHO and IC with a molar ratio of 1:2.
[b]Relative to IC group.
[c]The yields were determined by ^{1}H NMR spectroscopy (400 MHz) with toluene-d8 as an internal standard and solution.
[d]CDCl3 used as solvent, and 2 equiv. IC group was used.
[e]CDCl3 used as solvent, and 6 equiv. IC group was used.

chloride and carbon bromide (entries 15–16 in Table 2), they were found to be ineffective for this condensation, probably due to their poor capability in activating the aldehyde to form the diacetate intermediate. To better understand the high reaction activity of our method, we performed in situ NMR experiment for the conventional pyridine-catalyzed Knoevenagel condensation (Supplementary Fig. 5). With the adding of 2 eq IC and 1eq ITIC-CHO in the presence of pyridine, it can be seen that a lower conversion of 22% for ITIC was obtained after 12 h (entry 17 in Table 2). The result suggests that large excess of IC group is needed to push the equilibrium in favor of the final product in the conventional pyridine-catalyzed Knoevenagel condensation, confirming the high reaction activity of our $BF_3 \cdot OEt_2$-catalyzed method.

Then the effect of different anhydrides (Fig. 1b) on the reaction was examined (Fig. 1b, Supplementary Tables 2 and 3). As for the aliphatic carboxylic anhydrides (I-III), all reactions worked well for $GaCl_3$ and $BF_3 \cdot OEt_2$, albeit the anhydrides with longer alkyl chain (II) and steric alkyl chain (III) required slightly extended reaction time. Regarding the cyclic anhydrides (X, VIII and IV), only those with low ring strain can lead to the full completion of the reaction for $GaCl_3$ (Supplementary Table 2). While all of them are not effective for $BF_3 \cdot OEt_2$ (Supplementary Table 3). Our results indicate that aliphatic carboxylic anhydrides (I-III) are all potential candidates for the $BF_3 \cdot OEt_2$-catalyzed Knoevenagel condensation.

Mechanistic studies. The in situ ^{1}H NMR (Fig. 2) show the gradual consumption of starting materials (ITIC-CHO, IC), the presence of the diacetate intermediate and pre-product, as well as the formation of the product (ITIC). Initially, the disappearance of the proton at 9.40 ppm (the aldehyde of ITIC-CHO) and the appearance of new proton at 8.84 ppm (H3 in Fig. 2a) confirmed the complete conversion of ITIC-CHO to its corresponding diacetate. As the reaction progress, the intensity of H3 from the gem-diacetate decrease, while new germinal protons (assigned to the pre-product) at 8.77 ppm (H4) and 8.42 ppm (H5) show up with the same intensity. The final product was observed on the

basis of the new olefinic proton at 8.44 ppm (H7), and its intensity gradually increased with the disappearance of the typical protons for the intermediate and the pre-product. When the reaction turned to completion, the characteristic protons of the final product became the dominant peaks, suggestive of quantitative conversion of the starting materials to ITIC. The conclusion can also be supported by the evolution of the protons attached at the β-positions of the thiophene groups (HB2 from the diacetate at 7.97 ppm, HB3 from the pre-product at 7.94 ppm and HB4 from the product at 7.98 ppm), as a result of steric repulsion of the bulky groups attacked at the α-positions during the subsequent chemical transform.

Based on the above experiments and previous reports, the mechanism for the Lewis acid catalyzed one-pot reaction is illustrated in Fig. 2. Initially, the coordination of the carbonyl oxygen in ITIC-CHO with the Lewis acid generated a highly electrophilic carbonyl group, which was the primary driving force for such reaction. At this moment, significantly red shift was observed for the absorption of ITIC-CHO in toluene solution, suggestive of such coordination effect (Supplementary Fig. 4). Interestingly, the addition of THF or pyridine could lead to the recovery of its absorption, indicating the coordination of carbonyl group with Lewis acid was destroyed. This phenomenon could be used to explain the ineffectiveness of such condensation in THF or pyridine. Upon the coordination, the carbonyl group was attacked by the oxygen atom of acetic anhydride, and the subsequent intramolecular rearrangement gave the diacetate intermediate. Then, nucleophilic attack of the diacetate intermediate by the enolizable activated IC group led to the pre-product, which underwent elimination of acetic acid to afford the desired product along with release of the Lewis acid catalyst.

To gain more insights into the reaction, DFT calculations at the B3LYP/6-31G(d) level with the Gaussian 03 program package were carried out and the results are shown in Fig. 2d[41,42]. Notably, the reaction was simplified only with the consideration of the mono-aldehyde transformation for clarification, and thus F1 substrate was used as model compound for ITIC-CHO. In the Lewis acid-catalyzed pathway, it can be seen that converting aldehyde (F1) to the acylals intermediate (F2) is endothermic
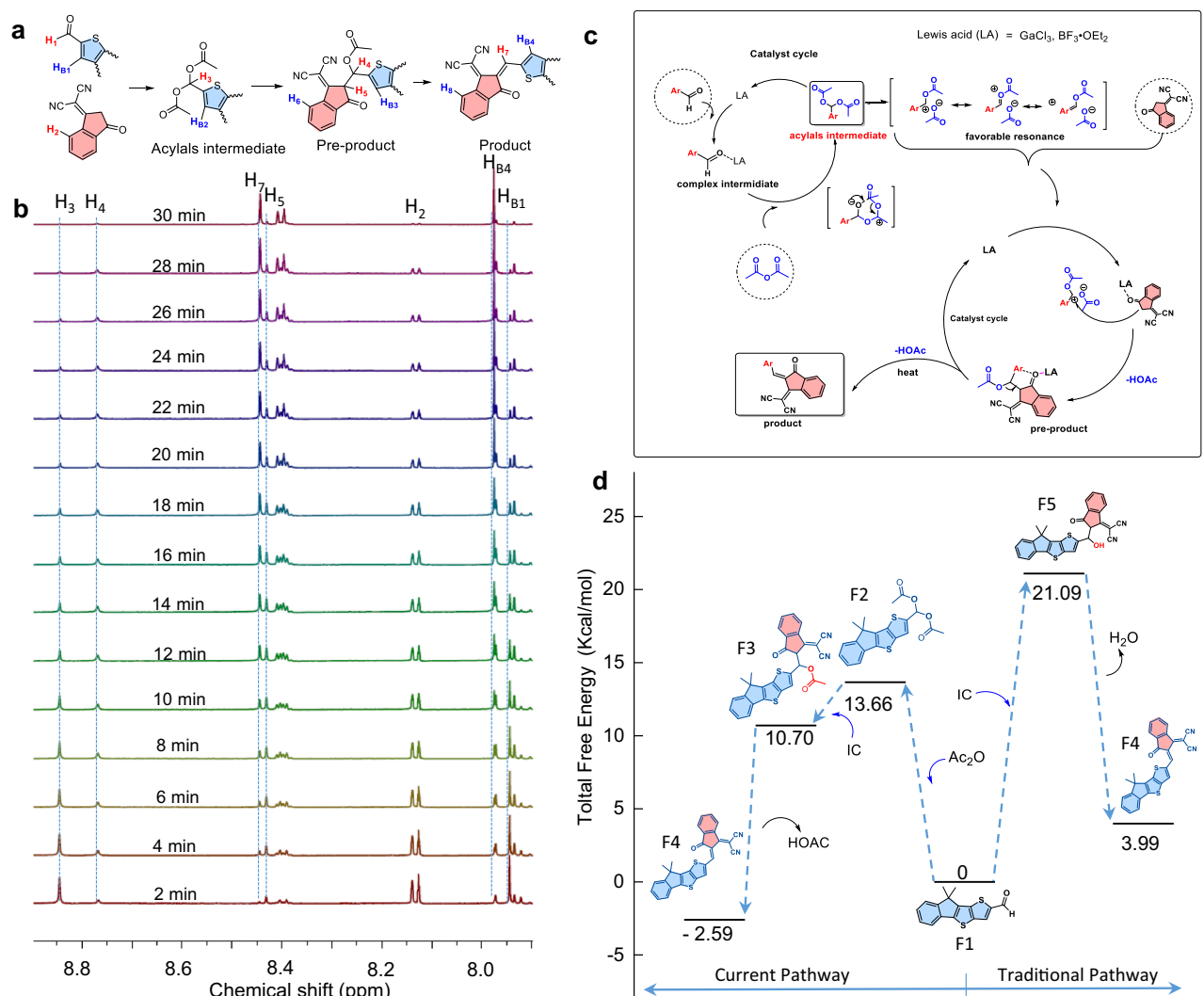
Fig. 2 Mechanism studies. a The reaction subsequently shows starting materials (ITIC-CHO, IC), the diacetate intermediate and pre-product, as well as the ITIC product. **b** In situ ^{1}H NMR (600 MHz) experiments in toluene-d_8 with an expanded view in the fields of 9.5-7.8 ppm. During the experiment, a mixture of ITIC-CHO (5.0 mg) and IC (1.8 mg) in a molar ratio of 1: 2 in toluene-d_8 (1 ml) was added into the NMR tube along with GaCl$_3$ (about 1 mg) and acetic anhydride (0.02 ml). **c** Plausible reaction pathways for the Lewis acid-catalyzed Knoevenagel condensation. **d** Computed free-energy profiles for comparison of the Lewis acid-catalyzed pathway and the traditional pathway. The calculation was conducted with B3LYP-6-31G (d, p). Relative Gibbs free energies of the reaction system at 298 K are given in kcal/mol, whereas the energy of the starting material is arbitrarily set to zero. In the molecules, the bule color represents D unit and the red color represents the A unit.

with a small energy barrier of 13.66 kcal mol^{-1}, and the subsequent sequence from acylal intermediate (F2) to the final product (F4) is highly thermodynamically favorable, with the total Gibbs energy change of the process being about −2.59 kcal mol^{-1}. However, in the conventional Knoevenagel condensation, the energy barrier to the alcohol intermediate (F5) was 21.09 kcal mol^{-1}, which makes it harder to overcome. And it is a classical reversible process with an endothermic energy barrier by 3.99 kcal mol^{-1} from aldehyde (F1) to the final product (F4). This might explain that large excess of IC-based methylene groups was required to push the equilibrium in favor of the final products for the conventional Knoevenagel condensation in the viewpoint of thermodynamics.

Scope of the method. With the newly established method in hand, we investigated the Knoevenagel condensation of various derivatives of ITIC-CHO with different side chains (and/or different aromatic-fused-rings) and the A units (Fig. 3). In general, the synthesis of all the SMAs were conducted in toluene at room

temperature for 15 min with BF$_3 \cdot$OEt$_2$ as catalyst. When the alkoxyl group (like IDD-CHO) incorporated in the side chains or thiadiazole groups in the aromatic-fused-rings (like Y6-CHO), all reactions proceeded smoothly to give the desired products. Besides those reported SMAs, the method is convenient for the construction of new SMAs, especially those with new A-end groups (Fig. 3c). As for the conventional pyridine-catalyzed Knoevenagel condensation, the acidity of the methylene group is also an important factor related to the yields of the reaction. Generally, the IC-based A groups (IC, Cl-IC and F-IC) have a higher degree of acidity than that of dione-base A groups (ID, Cl-ID, and F-ID), and the halide substitution on A groups can increase their degree of acidity. Interestingly, there is no obvious difference on the reactions when different A-units were used in the BF$_3 \cdot$OEt$_2$-catalyzed reactions (Fig. 3c). The result suggests that the BF$_3 \cdot$OEt$_2$-catalyzed Knoevenagel condensation is an effective approach for the synthesis of the SMAs.

Comparing with the classical pyridine-catalyzed Knoevenagel condensation, in which large excess of IC or its derivatives was
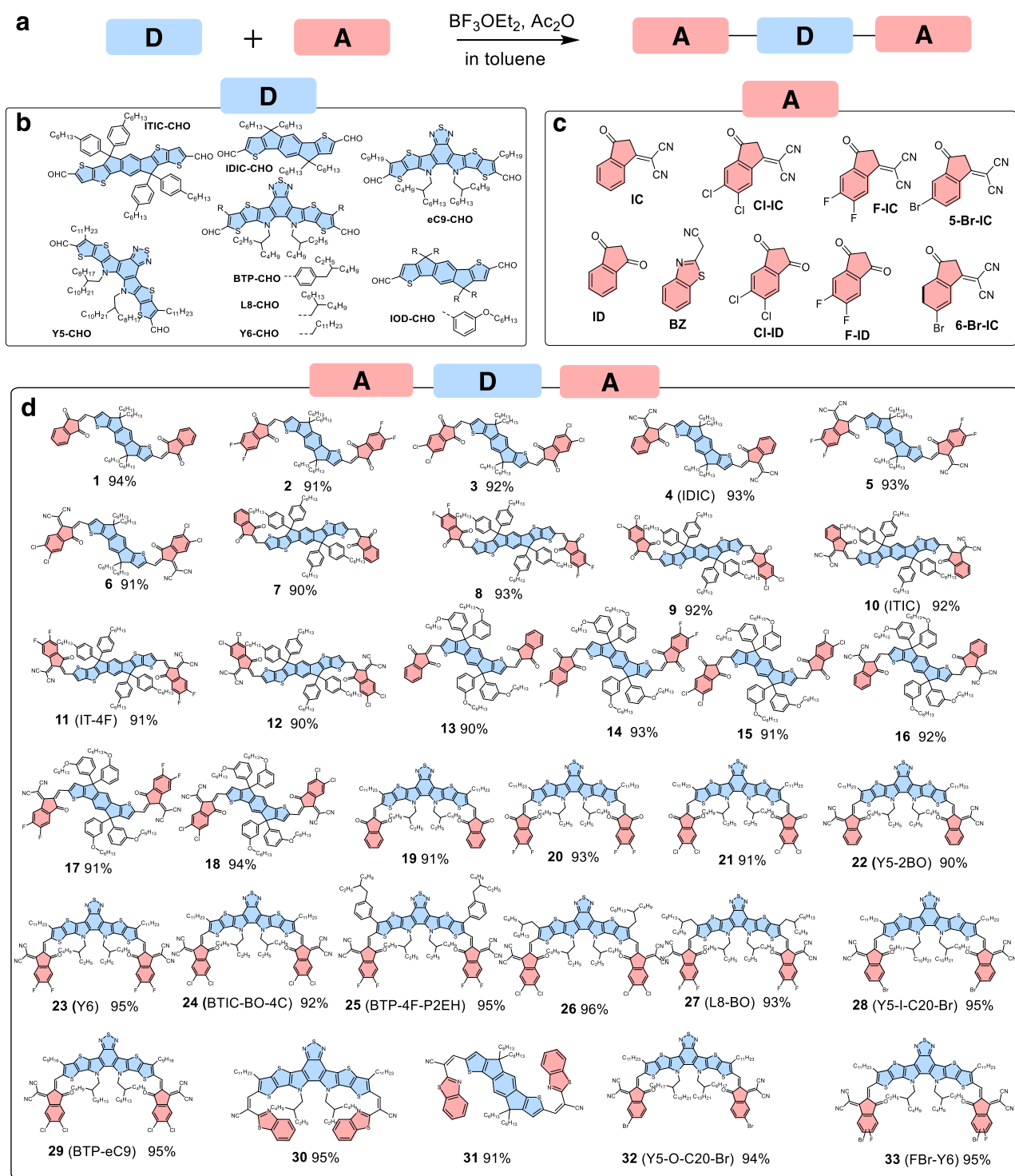
Fig. 3 Chemical structures and synthetic routes. a The synthetic route for SMAs; **b** The aldehyde-terminated D groups; **c** The end-capping A groups; **d** Chemical structures of SMAs generated with isolated yields. To simplify, here the D-units represent aromatic-fused-ring D or DA'D-core. In the molecules, the bule color represents D unit and the red color represents the A unit. For the reported SMAs, the abbreviations of their name are given in the brackets.

usually used to push the equilibrium in favor of the formation of the SMAs, our new method of the BF₃·OEt₂-catalyzed Knoevenagel condensation could quantitatively convert both starting materials to the corresponding products, providing an efficient and desirable approach for a low-cost synthesis of the SMAs, especially for those high-performance fluorinated ones, such as Y6 (**23**, in Fig. 3d). Recent studies revealed that

fluorinated SMAs could suppress nonradiative triplet loss to achieve a better device performance[43,44]. However, their conventional synthesis required the use of excessive costly fluorinated IC end groups (such as F-IC), which significantly impeded their real application. In addition, fluorinated IC (such as F-IC) exhibits higher reaction reactivity than its non-fluorinated counterpart (such as IC) due to the higher degree of acidity of the methylene

group. Thus they could further react with the target Knoevenagel SMA product, as evidenced by the synthesis of IT-4F using conventional pyridine-catalyzed Knoevenagel condensation (Supplementary Fig. 6). While using our $BF_3 \cdot OEt_2$-catalyzed Knoevenagel condensation, such phenomenon was not observed.

As a matter of fact, our new method of the $BF_3 \cdot OEt_2$-catalyzed Knoevenagel condensation could offer the pure final products through a simple reaction work-up, i.e., precipitation of the reaction mixture in methanol or ethanol followed by wash. Such a fast and quantitative transformation, together with its facile work-up, provide a convenient and economical procedure for a large-scale and low-cost preparation of the SMAs, which could potentially pave the way for their commercialization. As a typical example, a video of the synthesis of IT-4F (10, in Fig. 3d) is provided in Supplementary Video 1. To demonstrate this application, a gram-scale synthesis of Y6 was conducted with a high yield of 98%, while the initial reported yield of Y6 was only 64% at a miligram-scale[19] using classical pyridine-catalyzed Knoevenagel condensation. And the reaction is convenient for further scale-up if needed. With the model for cost calculation[45], the cost of material (C_g, cost-per-gram) for ITIC, IT-4F and Y6 obtained with our method are 164.8 \$ g^{-1}, and 192.3 \$ g^{-1} and 410.11 \$ g^{-1} (Supplementary Tables 5–7), all of which are thus reduced nearly by 50% relative to those using the conventional method. The result indicates that our modified strategy is helpful to provide low-cost photovoltaic acceptors for large-scale production.

Photovoltaic properties. For organic photovoltaic materials, besides their molecular structure, their purity is also an important factor determining the device performance. To improve the purity of SMAs, multiple column chromatography separations are needed in the conventional Knoevenagel condensation. This procedure is much more energy consuming, although they are effective to remove batch to batch variation in device performance. With the new method prepared SMAs (ITIC, IT-4F, FBr-Y6 and Y6) as acceptor, their photovoltaic performance was examined with PM6 or PBDB-T as donor (Fig. 4c). From Fig. 4 and Supplementary Table 8, it can be seen that all the SMAs show high PCE values, 10.66% for ITIC, 13.08% for IT-4F, 15.09% for FBr-Y6 and 17.15 % for Y6. The external quantum efficiency (EQE) spectra were measured to examine the spectral responses of the devices (Fig. 4d). The photo response range are related with optical bandgap of the SMAs, and the calculated short circuit current density (J_{SC}) values for the IPCE curves agree well with the J_{SC} values obtained from the J–V curves. For the SMAs of ITIC, IT-4F and Y6, their PCE values are comparable to those of their corresponding state-of-the-art devices reported in literatures[18,19,46]. The results further confirm that our $BF_3 \cdot OEt_2$-catalyzed reaction with the simple work-up procedure could provide the final product with good quality for the high-performance PSCs.

Discussion

A $BF_3 \cdot OEt_2$-catalyzed Knoevenagel condensation was developed for a fast and quantitative chemical synthesis of the A–D–A or A–DA'D–A structured SMAs, starting from aldehyde-terminated D or DA'D-units and end-capping A-units in the presence of acetic anhydride. Compared with the classical pyridine-catalyzed Knoevenagel condensation, this $BF_3 \cdot OEt_2$-catalyzed condensation provides a thermodynamically favored path to the synthesis of the SMAs in quantitative yields through the germinal diacetate intermediate at a low temperature, and a variety of SMAs were synthesized with a convenient work-up. A gram-scale
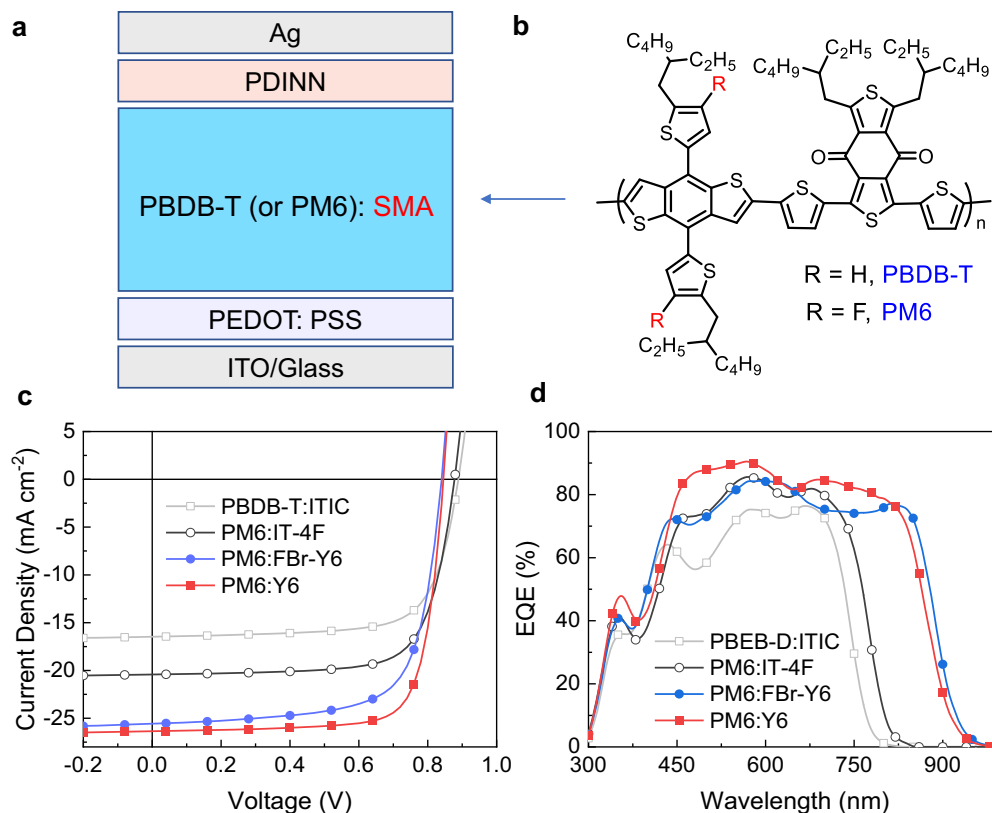

Fig. 4 Photovoltaic performance of the PSCs. a Device structure of the PSCs. **b** Chemical structure of polymer donors; **c** J–V curves of the best PSCs based on PM6: SMAs (ITIC, IT-4F, FBr-Y6 and Y6, synthesized by $BF_3 \cdot OEt_2$-catalyzed Knoevenagel condensation) blend under the illumination of AM 1.5 G, 100 mWcm^{-2}. **d** EQE spectra of the best devices.

preparation was also demonstrated for Y6, which could be about 50% cost-saving compared with conventional preparation. Furthermore, our results further confirm that the simple work-up procedure could provide the final product with good quality for the high-performance PSCs. The advantages of fast and quantitative transformation together with an easier workup make the BF₃·OEt₂-catalyzed Knoevenagel condensation as a convenient and greener procedure for a large-scale and low-cost preparation of the SMAs, which are desirable for commercialization of PSCs. Beside the application in SMAs, this method can be also applied to the low-cost synthesis of other photovoltaic donors, such as those D–A structured small molecular donors[30]. Thus the widely application of such methodology will certainly accelerate the commercialization of PSCs. As the Knoevenagel condensation is among the most fundamental and strategically important transformation to construct D–A semiconductors, this methodology also offers a modular and robust synthesis of tailed-made D–A conjugated organic and polymeric materials for a wide range of emerging technologies, such as thin film transistors, light-emitting diodes, as well as memory devices, and near infrared image sensors or chemotherapy.

Methods

Reagents and materials. Reaction progress was monitored using a thin-layer chromatography (glass backed, extra hard layer, 60 Å, 250 μm thickness, F254 indicator). All chemicals were obtained from commercially available sources and used without further purification. Solvents are used as received. All procedures were carried out under open atmosphere with no precautions taken to exclude ambient moisture. IC, Cl-IC, FBr-IC and Y6 (used as reference) were purchased from Shenzhen Yirou Photovoltaic Technology Co., Ltd (eFlexPV), and PM6 (used in device), ITIC-CHO, IDIC-CHO, IOD-CHO were purchased from Solarmer Materials. Y6-CHO was purchased from hyper. Inc. F-IC, F-ID, Cl-ID were purchased from SunTech Inc. ID and BZ were purchased from Bide Pharmatech Ltd. BTP-CHO, eC9-CHO, L8-CHO and Y5-CHO were synthesized according to the method of reference[47]. 5-Br-IC and 6-Br-IC were synthesized according to the method of references[48,49].

General producer for the synthesis of SMAs. The aldehyde-terminated D units (0.10 mmol) and the activated methylene based IC units (0.20 mmol) were dissolved in toluene (5 mL). BF₃·OEt₂ (5 equiv of the IC units) and acetic anhydride (0.1 ml) were added, and the reaction mixture was stirred at room temperature for 15 min. Then, the reaction mixture was added dropwise into methanol with stirring. The precipitate was collected, washed with methanol several times, then dissolved in chloroform and added dropwise into methanol again to afford product. This process was repeated several times until the target SMAs was pure enough for photovoltaic devices. While for other SMAs (2F-Ic-IOD, 2Cl-Ic-IOD, Ic-IOD, 2F-YT-IOD, 2Cl-YT-IOD and YT-IOD, structure in Fig. 3), ethanol was used instead of methanol. For the application in organic electronics, it is suggested that sufficient stirring of the SMAs precipitation must be ensured. Also, it is a straightforward procedure, just by filtration of the SMA solution (in dichloromethane) though a short pad of silica gel to avoid time-consuming stirring.

Gram-scale synthesis of Y6. The Y6-CHO (1.00 g, 0.95 mmol) and the F-IC (0.45 g, 0.47 mmol) were dissolved in toluene (30 mL). BF₃·OEt₂ (0.5 mL, 2.5 eq) and acetic anhydride (1.0 ml) were added, and the reaction mixture was stir at room temperature for 15 min. Then, the reaction mixture was dropwise into methanol, and the precipitate was collected as a crude product. The crude product was dissolved in chloroform and dropwise into methanol again to afford product (1.39 g, yield 98%).

Characterizations. Proton (¹H NMR) was recorded on Bruker AVQ-400 spectrometers using CDCl₃ or toluene-d₈ as solvents. While for the in situ experiment, ¹H NMR spectra were measured on a JNM-ECZ600R/S3 (Jeol, Japan) (600 MHz). Chemical shifts (δ) are referred to internal Me₄Si (0 ppm) as the standard, and are reported in ppm relative to the residual solvent signal (δ 7.26 for ¹H NMR in CDCl₃, δ 7.09, 7.00, 6.89 for ¹H NMR in toluene-d₈). Data for ¹H was reported as follows: chemical shift (δ ppm), multiplicity (s = singlet, d = doublet, t = triplet, q = quartet, quint = quintet, hept = heptet, m = multiplet, br = broad), coupling constant (Hz), integration. The yields were determined by ¹H NMR spectroscopy (400 MHz) in toluene-d₈ solvent, with its methyl group used as an internal standard to calculate the quantity of the substrates. This calculation is based on the ratio of the integrated peaks of aldehyde proton of the substrates (or the olefinic proton for SMA product) and the methyl group in toluene-d₈ solvent. The UV–vis absorption spectra were measured by Hitachi U-3010 UV–vis spectrophotometer.

Malid-tof-ms: MALDI measurements were performed with MALDI-TOF MS Bruker Autoflex II.

Device fabrication and characterization of the OSCs. The OSCs were fabricated with a structure of ITO/PEDOT: PSS/active layer/cathode interlayer (CIM)/Ag. The ITO glass was cleaned by sequential ultrasonic treatment in water, deionized water, acetone and isopropanol, and then treated in an ultraviolet ozone cleaner (Ultraviolet Ozone Cleaner, Jelight Company, USA) for 20 min. The PEDOT: PSS aqueous solution (Baytron P 4083 from H. C. Starck) was filtered through a 0.45 mm filter and then spin-coated on pre-cleaned ITO-coated glass at 4000 rpm for 30 s. Subsequently, the PEDOT: PSS film was annealed at 150 °C for 20 min in air to form a 30 nm film. A blend solution of PM6 or PBDB-T donor and SMA was prepared by dissolving the materials in chloroform, and then spin-coated at 4000 rpm onto the PEDOT: PSS layer. Then methanol solution of CIM (PDINN) at a concentration of 1.0 mg mL⁻¹ was deposited on the active layer at 3000 rpm for 30 s to afford a cathode buffer layer. Finally, the metal cathode Ag was thermal evaporated under a mask at a base pressure of approximately 10⁻⁵ Pa. The photovoltaic area of the device is 4.6 mm². Optical microscope (Olympus BX51) was used to define the active area of the devices. The current density-voltage (J-V) characteristics of the OSCs were measured in a nitrogen glove box with a Keithley 2450 Source Measure unit. Oriel Sol3A Class AAA Solar Simulator (model, Newport 94023A) with a 450 W xenon lamp and an air mass (AM) 1.5 filter was used as the light source. The light intensity was calibrated to 100 mW cm⁻² by a Newport Oriel 91150V reference cell. The voltage step and delay time were 10 mV and 1 ms, respectively. The scan started from −1.5 V to 1.5 V. The EQE was measured by Solar Cell Spectral Response Measurement System QE-R3-011 (Enli Technology Co., Ltd., Taiwan). The light intensity at each wavelength was calibrated with a standard single-crystal Si photovoltaic cell.

References
1. Yu, G., Gao, J., Hummelen, J. C., Wudl, F. & Heeger, A. J. Polymer photovoltaic cells: enhanced efficiencies via a network of internal donor-acceptor heterojunctions. *Science* **270**, 1789–1791 (1995).
2. Wadsworth, A. et al. Critical review of the molecular design progress in non-fullerene electron acceptors towards commercially viable organic solar cells. *Chem. Soc. Rev.* **48**, 1596–1625 (2019).
3. Yan, C. et al. Non-fullerene acceptors for organic solar cells. *Nat. Rev. Mater.* **3**, 18003 (2018).
4. Chen, H. et al. A guest-assisted molecular-organization approach for >17% efficiency organic solar cells using environmentally friendly solvents. *Nat. Energy* **6**, 1045–1053 (2021).
5. Li, C. et al. Non-fullerene acceptors with branched side chains and improved molecular packing to exceed 18% efficiency in organic solar cells. *Nat. Energy* **6**, 605–613 (2021).
6. Zhan, L. et al. Layer-by-layer processed ternary organic photovoltaics with efficiency over 18%. *Adv. Mater.* **33**, 2007231 (2021).
7. Chen, S. et al. High-performance polymer solar cells with efficiency over 18% enabled by asymmetric side chain engineering of non-fullerene acceptors. *Sci. China Chem.* **64**, 1192–1199 (2021).
8. Wang, J. et al. A tandem organic photovoltaic cell with 19.6% efficiency enabled by light distribution control. *Adv. Mater.* **33**, 2102787 (2022).
9. Zuo, L. et al. Dilution effect for highly efficient multiple-component organic solar cells. *Nat. Nanotech.* **17**, 53–60 (2022).
10. Chong, K. et al. Realizing 19.05% efficiency polymer solar cells by progressively improving charge extraction and suppressing charge recombination. *Adv. Mater.* **34**, 2109516 (2022).
11. Ma, X. et al. Approaching 18% efficiency of ternary organic photovoltaics with wide bandgap polymer donor and well compatible Y6: Y6-1O as acceptor. *Natl Sci. Rev.* **8**, nwaa305 (2020).
12. Cheng, P., Li, G., Zhan, X. & Yang, Y. Next-generation organic photovoltaics based on non-fullerene acceptors. *Nat. Photon* **12**, 131–142 (2018).
13. Hou, J., Inganäs, O., Friend, R. H. & Gao, F. Organic solar cells based on non-fullerene acceptors. *Nat. Mater.* **17**, 119 (2018).

14. Qian, D. et al. Design rules for minimizing voltage losses in high-efficiency organic solar cells. *Nat. Mater.* **17**, 703–709 (2018).

15. Hussain, M. D. W. et al. Design of nonfused nonfullerene acceptors based on pyrido- or benzothiadiazole cores for organic solar cells. *ACS Appl. Energy Mater.* **5**, 2202–2210 (2022).

16. Li, N., McCulloch, I. & Brabec, C. J. Analyzing the efficiency, stability and cost potential for fullerene-free organic photovoltaics in one figure of merit. *Energy Environ. Sci.* **11**, 1355–1361 (2018).

17. Sun, C. et al. A low cost and high performance polymer donor material for polymer solar cells. *Nat. Commun.* **9**, 743 (2018).

18. Lin, Y. et al. An electron acceptor challenging fullerenes for efficient polymer solar cells. *Adv. Mater.* **27**, 1170–1174 (2015).

19. Yuan, J. et al. Single-junction organic solar cell with over 15% efficiency using fused-ring acceptor with electron-deficient core. *Joule* **3**, 1140–1151 (2019).

20. Chai, G. et al. Fine-tuning of side-chain orientations on nonfullerene acceptors enables organic solar cells with 17.7% efficiency. *Energy Environ. Sci.* **14**, 3469–3479 (2021).

21. Huang, J., Tang, H., Yan, C. & Li, G. 1,1-Dicyanomethylene-3-indanone end-cap engineering for fused-ring electron acceptor-based high-performance organic photovoltaics. *Cell. Rep. Phys. Sci.* **2**, 100292 (2021).

22. Lin, F., Jiang, K., Kaminsky, W., Zhu, Z. & Jen, A. K. Y. A non-fullerene acceptor with enhanced intermolecular π-core interaction for high-performance organic solar cells. *J. Am. Chem. Soc.* **142**, 15246–15251 (2020).

23. Yuan, J. et al. Enabling low voltage losses and high photocurrent in fullerene-free organic photovoltaics. *Nat. Commun.* **10**, 570 (2019).

24. Chen, Y., Zheng, Y., Jiang, Y., Fan, H. & Zhu, X. Carbon-bridged 1,2-Bis(2-thienyl)ethylene: an extremely electron rich dithiophene building block enabling electron acceptors with absorption above 1000 nm for highly sensitive NIR photodetectors. *J. Am. Chem. Soc.* **143**, 4281–4289 (2021).

25. Li, G. et al. Systematic merging of nonfullerene acceptor π-extension and tetrafluorination strategies affords polymer solar cells with >16% efficiency. *J. Am. Chem. Soc.* **143**, 6123–6139 (2021).

26. Dai, S. et al. Fused nonacyclic electron acceptors for efficient polymer solar cells. *J. Am. Chem. Soc.* **139**, 1336–1343 (2017).

27. Lai, H. et al. Trifluoromethylation enables a 3D interpenetrated low-band-gap acceptor for efficient organic solar cells. *Joule* **4**, 688–700 (2020).

28. Luo, Z. et al. Fine-tuning of molecular packing and energy level through methyl substitution enabling excellent small molecule acceptors for nonfullerene polymer solar cells with efficiency up to 12.54%. *Adv. Mater.* **30**, 1706124 (2018).

29. Yao, H. et al. Design, synthesis, and photovoltaic characterization of a small molecular acceptor with an ultra-narrow band gap. *Angew. Chem. Int. Ed.* **56**, 3045–3049 (2017).

30. Wan, X., Li, C., Zhang, M. & Chen, Y. Acceptor–donor–acceptor type molecules for high performance organic photovoltaics – chemistry and mechanism. *Chem. Soc. Rev.* **49**, 2828–2842 (2020).

31. Jones, G. The knoevenagel condensation. In *Organic reactions*. 204–599 (John Wiley & Sons, Inc., 2011).

32. Bürckstümmer, H. et al. Efficient solution-processed bulk heterojunction solar cells by antiparallel supramolecular arrangement of dipolar donor–acceptor dyes. *Angew. Chem. Int. Ed.* **50**, 11628–11632 (2011).

33. Kochhar, K. S., Bal, B. S., Deshpande, R. P., Rajadhyaksha, S. N. & Pinnick, H. W. Protecting groups in organic synthesis. Part 8. Conversion of aldehydes into geminal diacetates. *J. Org. Chem.* **48**, 1765–1767 (1983).

34. Sumida, N., Nishioka, K. & Sato, T. Conversion of aldehydes into geminal dicarboxylates (acylals) catalyzed by lithium tetrafluoroborate. *Synlett*, **2001**, 1921–1922 (2001).

35. Karimi, B. & Maleki, J. Lithium trifluoromethanesulfonate (LiOTf) as a recyclable catalyst for highly efficient acetylation of alcohols and diacetylation of aldehydes under mild and neutral reaction conditions. *J. Org. Chem.* **68**, 4951–4954 (2003).

36. Ogiwara, Y., Takahashi, K., Kitazawa, T. & Sakai, N. Indium(III)-catalyzed knoevenagel condensation of aldehydes and activated methylenes using acetic anhydride as a promoter. *J. Org. Chem.* **80**, 3101–3110 (2015).

37. Schopp, N. et al. Effect of Palladium-Tetrakis(Triphenylphosphine) catalyst traces on charge recombination and extraction in non-fullerene-based organic solar cells. *Adv. Funct. Mater.* **31**, 2009363 (2021).

38. Nikiforov, M. P. et al. Detection and role of trace impurities in high-performance organic solar cells. *Energy Environ. Sci.* **6**, 1513–1520 (2013).

39. Amemiya, R. & Yamaguchi, M. GaCl₃ in organic synthesis. *Eur. J. Org. Chem.* **2005**, 5145–5150 (2005).

40. Yamaguchi, M., et al. Gallium Trichloride. In *Encyclopedia of Reagents for Organic Synthesis*. 1–8 (John Wiley &Sons, Inc., 2014).

41. Lee, C. T., Yang, W. T. & Parr, R. G. Development of the colle-salvetti correlation-energy formula into a functional of the electron-density. *Phys. Rev. B* **37**, 785–789 (1988).

42. Frisch, M. J., et al. *Gaussian 09, revision B. 01* (Wallingford, CT, 2009).

43. Wang, R. et al. Nonradiative triplet loss suppressed in organic photovoltaic blends with fluoridated nonfullerene acceptors. *J. Am. Chem. Soc.* **143**, 4359–4366 (2021).

44. Gillett, A. J. et al. The role of charge recombination to triplet excitons in organic solar cells. *Nature* **597**, 666–671 (2021).

45. Li, X. et al. Simplified synthetic routes for low cost and high photovoltaic performance n-type organic semiconductor acceptors. *Nat. Commun.* **10**, 519 (2019).

46. Li, W. et al. A high-efficiency organic solar cell enabled by the strong intramolecular electron push–pull effect of the nonfullerene acceptor. *Adv. Mater.* **30**, 1707170 (2018).

47. Zhang, J. et al. Alkyl-chain branching of non-fullerene acceptors flanking conjugated side groups toward highly efficient organic solar cells. *Adv. Energ. Mater.* **11**, 2102596 (2021).

48. Luo, Z. et al. Precisely controlling the position of bromine on the end group enables well-regular polymer acceptors for all-polymer solar cells with efficiencies over 15%. *Adv. Mater.* **32**, 2005942 (2020).

49. Qu, J. et al. Bromination of the small-molecule acceptor with fixed position for high-performance solar cells. *Chem. Mater.* **31**, 8044–8051 (2019).

Author contributions

Z.G.Z. and Y.L. supervised the project. Z.G.Z. and H.F. designed the experiments, and H.F. conducted the experiments for the SMAs. L.X. and S.L. synthesized Y6-CHO. Q.Z. provide the in situ NMR experiments, J.Y., M.Z., and L.M. carried out the device characterization, and analyzed the device parameters. H.F. and M.L. conducted the DFT calculations. Z.G.Z., and H.F. wrote the paper, and Y.L. revised the manuscript.

Competing interests

The authors declare no competing interests.

Additional information

Supplementary information The online version contains supplementary material available at https://doi.org/10.1038/s41467-022-31389-y.

Correspondence and requests for materials should be addressed to Zhi-Guo Zhang.

Peer review information *Nature Communications* thanks Hyosung Choi, and the other, anonymous, reviewers for their contribution to the peer review of this work.

Reprints and permission information is available at http://www.nature.com/reprints

Publisher's note Springer Nature remains neutral with regard to jurisdictional claims in published maps and institutional affiliations.